# High $H_2$ Sorption Energetics in Zeolitic Imidazolate Frameworks

Tony Pham,[†,§] Katherine A. Forrest,[†,§] Hiroyasu Furukawa,[∥,⊥] Margarita Russina,[‡] Alberto Albinati,[○] Juergen Eckert,[*,†] and Brian Space[*,†]

[†]*Department of Chemistry, University of South Florida, 4202 East Fowler Avenue, CHE205, Tampa, FL 33620-5250, United States*

[∥]*Department of Chemistry, University of California-Berkeley, Materials Sciences Division, Lawrence Berkeley National Laboratory, Berkeley, CA, 94720, United States*

[⊥]*Center of Research Excellence in Nanotechnology (CENT), King Fahd University of Petroleum and Minerals, Dhahran 34464, Saudi Arabia*

[‡]*Helmholtz-Zentrum Berlin, für Materialien und Energie, Lise-Meitner Campus, Hahn-Meitner-Platz 1, 14109 Berlin, Germany*

[○]*Department of Structural Chemistry, University of Milan, 21 Via G. Venezian, I-20133 Milan, Italy*

**ABSTRACT:** A combined experimental and theoretical study of $H_2$ sorption was carried out on two isostructural zeolitic imidazolate frameworks (ZIFs), namely ZIF-68 and ZIF-69. The former consists of $Zn^{2+}$ ions that are coordinated to two 2-nitroimidazolate and two benzimidazolate linkers in a tetrahedral fashion, while 5-chlorobenzimidazolate is used in place of benzimidazolate in the latter compound. $H_2$ sorption measurements showed that the two ZIFs display similar isotherms and isosteric heats of adsorption ($Q_{st}$). The experimental initial $H_2$ $Q_{st}$ value for both ZIFs was determined to be 8.1 kJ mol$^{-1}$, which is quite high for materials that do not contain exposed metal centers. Molecular simulations of $H_2$ sorption in ZIF-68 and ZIF-69 confirmed the similar $H_2$ sorption properties between the two ZIFs, but also suggest that $H_2$ sorption is slightly favored in ZIF-68. This work also presents inelastic neutron scattering (INS) spectra for $H_2$ sorbed in ZIFs for the first time. The spectra for ZIF-68 and ZIF-69 shows a broad range of intensities starting from about 4 meV. The most favorable $H_2$ sorption site in both ZIFs correspond to a confined region between two adjacent 2-nitroimidazolate linkers. Two-dimensional quantum rotation calculations for $H_2$ sorbed at this site in ZIF-68 and ZIF-69 produced rotational transitions that are in accord with the lowest energy peak observed in the INS spectrum for the respective ZIFs. We found that the primary binding site for $H_2$ in the two ZIFs generates high barriers to rotation for the adsorbed $H_2$, which are greater than those in several metal–organic frameworks (MOFs) which possess open-metal sites. $H_2$ sorption was also observed for both ZIFs in the vicinity of the nitro groups of the 2-nitroimidazolate linkers. This study highlights the constructive interplay of experiment and theory to elucidate critical details of the $H_2$ sorption mechanism in these two isostructural ZIFs.

## I. INTRODUCTION

Metal–organic frameworks (MOFs) are an increasingly important class of crystalline materials that have shown considerable promise for a number of energy related applications, with one of the most notable applications being the storage of $H_2$.[1–3] MOFs are synthesized by combining metal ions with organic bridging ligands; the resulting structure is a porous three-dimensional material which can adsorb a variety of guest molecules including molecular $H_2$.[4] MOFs offer many promising features and advantages over traditional materials for $H_2$ storage, such as the ability of adsorbing $H_2$ and releasing it quickly by minor adjustments of thermodynamic conditions. However, one of the principal challenges to the eventual use of MOFs as a $H_2$ storage medium is the necessity to store large amounts of $H_2$ at moderate pressures and ambient temperatures.[1–3] Indeed, the maximum reported uptake of $H_2$ in numerous extant MOFs is no greater than 1.5 wt % at room temperature and high pressures (e.g., 100 atm). The ultimate U.S. Department of Energy (DOE) target for an on-board hydrogen storage system is 7.5 wt % under such conditions.[5] In order to improve room temperature $H_2$ sorption in MOFs, future research must focus on increasing the $H_2$ adsorption enthalpy between the framework and the $H_2$ molecules.[1–3] A $H_2$ adsorption enthalpy in the range of 15–30 kJ mol$^{-1}$ has been estimated to be necessary for adequate room temperature $H_2$ storage in MOFs.[6,7]

Different MOFs can be synthesized by varying the metal ion and/or ligand set.[8,9] The combination of various transition metal ions (e.g., $Zn^{2+}$, $Co^{2+}$) with imidazolate-type ligands have led to the design and synthesis of a subclass of MOFs called zeolitic imidazolate frameworks (ZIFs).[10–18] The metal ion in these materials represents a tetrahedral node in the structure. Different kinds of imidazolate-type ligands have been used to construct ZIFs, such imidazolate, 2-methylimidazolate, and benzimidazolate, which can result in distinct topologies that are similar to those found in inorganic zeolites. Recent experimental studies have shown that ZIFs hold great promise for a variety of gas sorption applications,[12,14–16,19–24] and that they exhibit remarkable chemical and thermal stability because of the presence of saturated metal centers.[12,14] This is the reason why ZIFs have greater relevance for industrial applications in gas sorption and separation than most other types of MOFs. Apart from the experimental studies, numerous theoretical studies have been performed on ZIFs to gain insight into the gas sorption and separation mechanisms in these materials.[21–34]

While most of the recent experimental and theoretical studies on ZIFs have focused on $CO_2$ sorption and separation, very few studies of $H_2$ sorption in these materials have

been reported.[12,13,19,27] Park *et al.* performed what appears to be the first experimental adsorption measurements of $H_2$ in ZIFs, where the authors reported isotherms on ZIF-8 and ZIF-11.[12] They determined a $H_2$ uptake capacity of 12.9 and 13.7 mg $g^{-1}$ for ZIF-8 and ZIF-11, respectively, at 77 K and 1.0 atm. ZIF-8 was also found to adsorb 31 mg $g^{-1}$ of $H_2$ at 77 K and 55 bar. Wu *et al.* provided the first molecular level study to gain insights into the ZIF–$H_2$ interaction using neutron powder diffraction (NPD) for $H_2$ adsorbed in the prototypical ZIF-8 material.[19] The authors found that $H_2$ molecules primarily bind onto the imidazolate linkers in this ZIF. These findings were later confirmed by grand canonical Monte Carlo (GCMC) simulations of $H_2$ sorption in ZIF-8.[27]

In this work we report a combined experimental and theoretical study of $H_2$ adsorption in ZIF-68 and ZIF-69, two isostructural ZIFs with **gme** (gmelinite) topology.14. ZIF-68 consists of $Zn^{2+}$ ions coordinated to two 2-nitroimidazolate and two benzimidazolate ligands in a tetrahedral fashion (Figure 1(a)). In ZIF-69, the benzimidazolate ligands are replaced by 5-chlorobenzimidazolate (Figure 1(b)). The overall structures of ZIF-68 and ZIF-69 are depicted in Figures 1(c) and 1(d), respectively. These ZIFs were originally investigated for their $CO_2$ sorption properties, where it was found that ZIF-69 displays higher $CO_2$ uptake and selectivity than ZIF-68.[14,16] This finding was later verified through GCMC simulations of $CO_2$ sorption and separation in the respective ZIFs.[28] The better $CO_2$ sorption properties of ZIF-69 relative to those of ZIF-68 likely arise from the presence of the electronegative chlorine atoms in the former, which can interact favorably with the $CO_2$ molecules.

In contrast to the case for $CO_2$, we find that ZIF-68 and ZIF-69 display similar sorption characteristics for $H_2$. To the best of our knowledge, this study reports experimental $H_2$ sorption isotherms and isosteric heats of adsorption ($Q_{st}$) in ZIF-68 and ZIF-69 for the first time. The experimental $H_2$ adsorption isotherms at 77 and 87 K were found to be similar for both ZIFs at the respective temperatures. The $Q_{st}$ values for $H_2$ are also nearly identical between the two ZIFs for all loadings considered, especially at zero-loading. The experimental initial $H_2$ $Q_{st}$ value for both ZIFs was determined to be 8.1 kJ $mol^{-1}$, which is higher than that for a number of existing MOFs, including those that contain open-metal sites.[3]

We performed GCMC simulations of $H_2$ adsorption in ZIF-68 and ZIF-69 to verify the experimental finding that the two ZIFs display similar $H_2$ sorption properties. Accurate molecular level predictions on the $H_2$ sorption mechanism can be made from the simulations if good agreement with experiment is obtained, such as insights into the reason for the high $H_2$ adsorption enthalpy in both ZIFs. Molecular simulations were also used to identify the favorable $H_2$ sorption sites in ZIF-68 and ZIF-69. It will be revealed that there is a sorption site present in both ZIFs that is responsible for the high experimental initial $H_2$ $Q_{st}$ values.

We also carried out inelastic neutron scattering (INS) studies of $H_2$ adsorbed in ZIF-68 and ZIF-69 to obtain molecular level information on the binding sites in the respective ZIFs. While Wu *et al.* reported the first and only NPD study of the locations of $H_2$ sorbed in a ZIF,[19] this work reports the INS spectra for $H_2$ sorbed in such materials for the first time to the best of our knowledge. INS is a powerful spectroscopic technique that is used to gain insights into the energetics and rotational barriers for $H_2$ sorbed in various porous materials, including MOFs.[35,36] The INS spectra for adsorbed $H_2$ usually consist of a number of different peaks from transitions of the hindered $H_2$ rotor, where each rotational tunnelling transition corresponds to $H_2$ sorbed at a specific site in the host. Rotational tunnelling transitions at lower energies correspond to a higher barrier to rotation, and therefore, a stronger interaction with the material.

A detailed analysis of the INS spectra is made by way of quantum dynamics calculations within a given potential en-

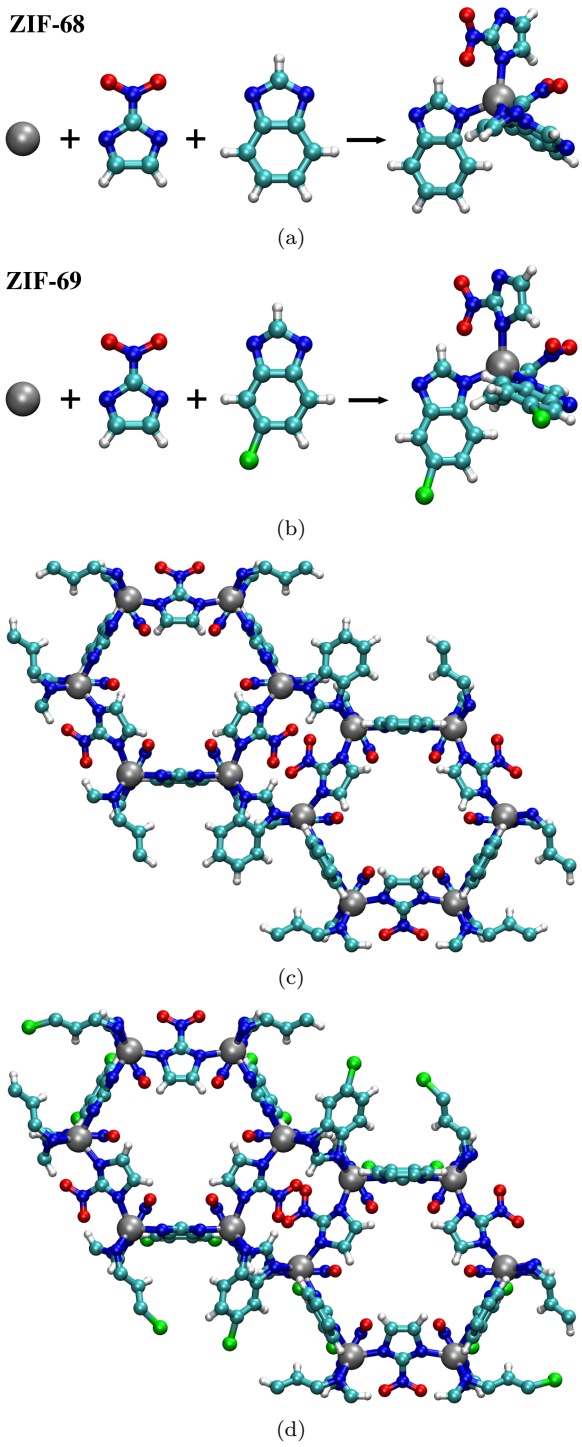


**Figure 1.** **(a)** and **(b)** show the scheme for the assembly of the tetrahedral node in ZIF-68 (using $Zn^{2+}$, 2-nitroimidazolate, and benzimidazolate) and ZIF-69 (using $Zn^{2+}$, 2-nitroimidazolate, and 5-chlorobenzimidazolate), respectively. **(c)** and **(d)** show the orthographic *c*-axis view of the unit cell of ZIF-68 and ZIF-69, respectively. Atom colors: C = cyan, H = white, N = blue, O = red, Cl = green, Zn = silver.

ergy surface.[36] Thus, we performed two-dimensional quantum rotation calculations for $H_2$ adsorbed at different sites that were identified from our simulations in both ZIFs. We will show that our calculated $j = 0$ to $j = 1$ transition energies for such sites in ZIF-68 and ZIF-69 correspond to a region in the INS spectrum of both ZIFs, which are very broad. The rotational barriers calculated for $H_2$ at the most favorable binding site in both ZIFs are higher than those for a number of extant MOFs, even some that possess open-metal sites.

## II. METHODS

### A. Experimental Section

ZIF-68 and ZIF-69 were synthesized and activated according to the procedure reported in reference 14. The experimental $H_2$ sorption isotherms for both ZIFs at 77 and 87 K and pressures up to 800 mmHg were measured using the Autosorb-1 (Quantachrome) volumetric analyzer. The experimental $H_2$ $Q_{st}$ values for ZIF-68 and ZIF-69 were determined for a range of loadings by applying the virial method[37,38] to the corresponding experimental isotherms at 77 and 87 K. The experimental INS spectrum for ZIF-68 and ZIF-69 were collected on the cold neutron time-of-flight spectrometer NEAT at the reactor of the Berlin Neutron Science Center using 1.1 and 0.8 g of the activated sample, respectively. Adsorption of $H_2$ in an amount corresponding to 2 molecules per formula unit was carried out *in situ* at 77 K from an external gas handling system into the evacuated sample cell, and the INS spectrum was collected at a temperature of 5 K. The incident wavelength that was chosen in these measurements was 2.1 Å such that the necessary energy transfer could be reached by neutron energy loss.

### B. Theoretical Section

Simulations of $H_2$ adsorption in ZIF-68 and ZIF-69 were performed by GCMC methods[39] in a unit cell of the individual ZIFs as shown in Figure 1(c) and 1(d), respectively. More details are provided in the Supporting Information (see Grand Canonical Monte Carlo section). The single X-ray crystallographic structures for the two ZIFs 14 were used for the parametrizations and simulations in this work. All ZIF atoms were kept fixed at their crystallographic positions throughout the simulations.

The global minimum (i.e., the most favorable sorption site) for $H_2$ in the respective ZIF was determined by simulated annealing[40] within the canonical ensemble ($NVT$) of a single $H_2$ molecule in a unit cell of ZIF-68 and ZIF-69. The simulations started at an initial temperature of 1,000 K and this temperature was scaled by a factor of 0.99999 after every 1,000 Monte Carlo steps. The simulations continued until the temperature of the system dropped below 2.5 K.

The total potential energy of ZIF–$H_2$ system is given by the sum of repulsion/dispersion, permanent electrostatic, and many-body polarization energies. These were calculated using the Lennard-Jones 12–6 potential, partial charges with Ewald summation,[41,42] and a Thole-Applequist type model,[43–46] respectively. All atoms of ZIF-68 and ZIF-69 were assigned Lennard-Jones parameters ($\epsilon$ and $\sigma$), point partial charges, and point polarizabilities to model the corresponding interactions. Details of obtaining these parameters for the ZIF atoms are provided in the Supporting Information (see Repulsion/Dispersion and Polarizability Parameters, Partial Charges For ZIF-68 and Partial Charges For ZIF-69 sections). Quantum mechanical dispersion effects were included semiclassically by way of Feynman-Hibbs corrections to the fourth order[47] for simulations at the temperatures considered herein (77 and 87 K).

Four different $H_2$ potentials with varying complexities were considered in this work: the single–site Lennard-Jones model developed by V. Buch,[48] the three–site electrostatic model developed by Darkrim and Levesque,[49] the five–site electrostatic model developed by Belof *et al.*,[50] and the five–site polarizable model also developed by Belof *et al.*[50] These models are denoted Buch, DL, BSS, and BSSP, respectively. The simulated results are presented for the polarizable potential; however, the simulated $H_2$ sorption isotherms and $Q_{st}$ values for the other models in both ZIFs are discussed where appropriate, with data shown in the Supporting Information (Figures S6 and S12).

Two-dimensional quantum rotation calculations were carried out for $H_2$ adsorbed at certain sites in ZIF-68 and ZIF-69 that were determined from the simulations. This method involves solving the rigid rotor Hamiltonian for the ZIF–$H_2$ system, with the sorbate molecule positioned at a particular site in the crystallographic unit cell of the host, to obtain the rotational energy levels for the perturbed $H_2$ molecule. More details on the quantum rotation calculations are provided in the Supporting Information (see Quantum Rotation Calculations section).

The rotational potential energy surface (PES) for $H_2$ sorbed at the most favorable site in both ZIFs was calculated to gain insights into the barrier to rotation that it is subject to. The total potential energy of the ZIF–$H_2$ system was calculated as the $H_2$ molecule was rotated at various angles of $\theta$ (0–180°) and $\phi$ (0–360°), with the center-of-mass of the sorbate kept fixed to map out the potential energy surface. The barrier to rotation was determined from the difference between the highest and lowest values on the rotational PES, which is projected onto the surface of a sphere.

## III. RESULTS AND DISCUSSION

### A. Isotherms and Isosteric Heats of Adsorption

The experimental $H_2$ sorption isotherms in ZIF-68 and ZIF-69 at 77 and 87 K and pressures up to 800 mmHg are shown in Figure 2. The $H_2$ uptake capacity for ZIF-68 and ZIF-69 at 77 K and 1.0 atm was determined to be 13.1 and 12.3 mg $g^{-1}$, respectively, whereas such values at 87 K and 1.0 atm were measured to be 8.8 and 8.7 mg $g^{-1}$ for the respective ZIFs. A direct comparison of the experimental $H_2$ sorption isotherms for the two ZIFs at both temperatures is shown in the Supporting Information (Figure S5(a)). Overall, ZIF-68 and ZIF-69 were found to have similar $H_2$ sorption isotherms for the considered pressure range at both 77 and 87 K. The relevant $H_2$ adsorption data and experimental properties for both ZIFs are summarized in Table 1.

Comparisons of the simulated $H_2$ adsorption isotherms for the four different $H_2$ potentials with the corresponding experimental measurements in ZIF-68 and ZIF-69 at 77 and 87 K are shown in the Supporting Information (Figures S6(a)–S6(b) and S12(a)–S12(b)). Simulations using the polarizable

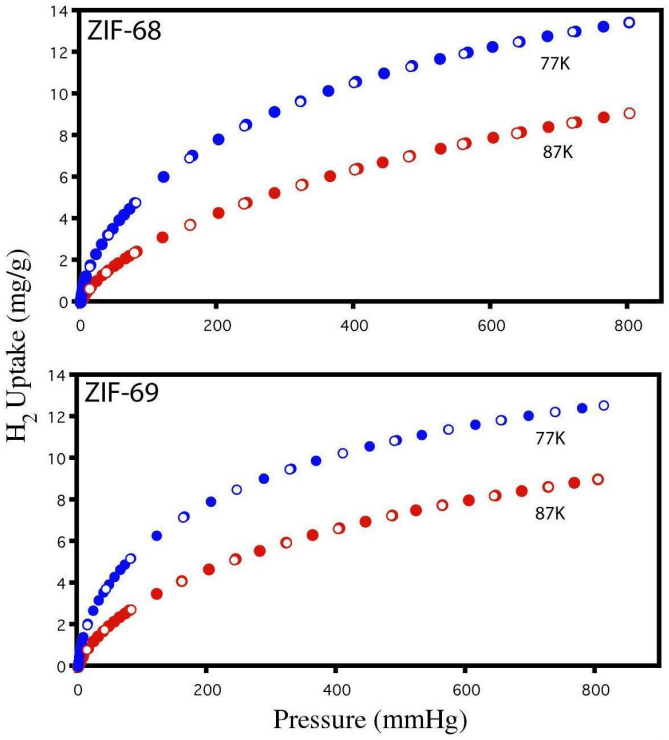


**Figure 2.** Experimental $H_2$ sorption isotherms for ZIF-68 (top) and ZIF-69 (bottom) at 77 K (blue) and 87 K (red). Adsorption is shown in closed symbols, while desorption is shown in open symbols.

BSSP model produced isotherms that are in excellent agreement with experiment to within joint uncertainties in ZIF-68 for all pressures considered at both temperatures (Figures S6(a)–S6(b)). The isotherms generated by the DL model slightly oversorb relative to the experimental results under these conditions. The BSS model resulted in uptakes that are slightly lower than those for the analogous polarizable model at the state points considered, while those for the single–site Buch model were the lowest in ZIF-68 at all state points considered, with isotherms that significantly undersorb experiment at both temperatures.

In the case of ZIF-69, the BSSP model generated uptakes that are slightly lower than experiment starting at 0.20 atm at both temperatures (Figures S12(a)–S12(b)). Otherwise, the isotherms obtained using this model are in good agreement with experiment to within joint uncertainties. Simulations using the DL model produced isotherms that essentially match the experimental data across all pressures at 77 and 87 K. We note that while the DL model is widely used in simulations studies of $H_2$ adsorption in MOFs, it can produce aberrant results in certain cases.[51–54] The same trends that were observed for the BSS and Buch models in ZIF-68 are also seen for ZIF-69.

Our simulations suggest that the $H_2$ uptake by ZIF-68 is somewhat higher than that in ZIF-69 at 77 K/1.0 atm and 87 K/1.0 atm regardless of which $H_2$ potential was used; this is consistent with experimental observation. This could result from the larger $d_a$ and $d_p$ values for ZIF-68 (see Table 1), which may allow for greater accommodation of $H_2$ molecules at higher pressures. The greater density of ZIF-69, resulting from the presence of the heavy Cl atoms in the structure, may also explain why ZIF-69 adsorbs less $H_2$ than ZIF-68 under such conditions.

Even though the uptake of $H_2$ in ZIF-68 is slightly higher

**Table 1.** Summary of the experimental properties and $H_2$ sorption data for ZIF-68 and ZIF-69. The Langmuir and BET surface areas for both ZIFs were taken from reference 14 and 17, respectively. $d_a$ and $d_p$ are defined as the diameter of the largest sphere that will pass through the pore and fit into the cavities, respectively.[14]

| ZIF | ZIF-68 | ZIF-69 |
|---|---|---|
| Langmuir Surface Area ($m^2$ $g^{-1}$) | 1220 | 1070 |
| BET Surface Area ($m^2$ $g^{-1}$) | 1090 | 950 |
| Density (g $cm^{-3}$) | 1.047 | 1.295 |
| $d_a$ (Å) | 7.5 | 10.3 |
| $d_p$ (Å) | 4.4 | 7.8 |
| $H_2$ Uptake at 77 K/0.10 atm (mg $g^{-1}$) | 4.5 | 4.9 |
| $H_2$ Uptake at 77 K/1.0 atm (mg $g^{-1}$) | 13.1 | 12.3 |
| $H_2$ Uptake at 87 K/0.10 atm (mg $g^{-1}$) | 2.2 | 2.6 |
| $H_2$ Uptake at 87 K/1.0 atm (mg $g^{-1}$) | 8.8 | 8.7 |
| Initial $H_2$ $Q_{st}$ (kJ $mol^{-1}$) | 8.1 | 8.1 |

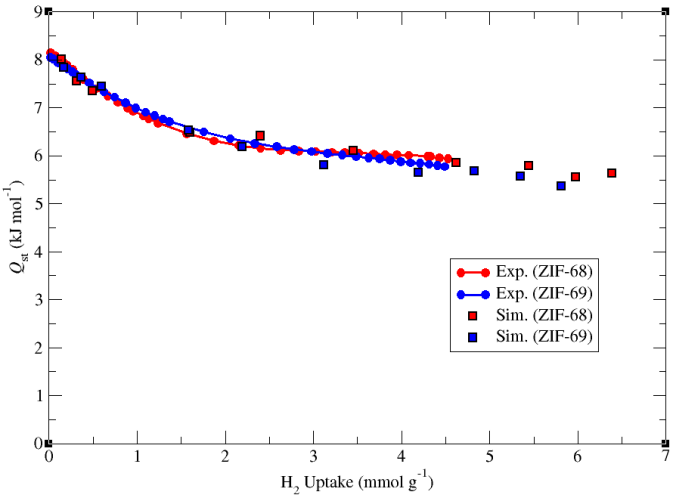


**Figure 3.** Isosteric heat of adsorption ($Q_{st}$) for $H_2$ in ZIF-68 (red) and ZIF-69 (blue) plotted against $H_2$ uptakes for experiment (circle) and simulation (square). The simulated results were obtained using the polarizable $H_2$ potential.[50]

than that in ZIF-69 at 77 K/1.0 atm and 87 K/1.0 atm according to both experiment and simulation, the experimental data shows that the $H_2$ uptake is somewhat higher for ZIF-69 in the low pressure region at both temperatures. The experimental $H_2$ uptake for ZIF-69 at 0.10 atm is 0.4 mg $g^{-1}$ higher than that in ZIF-68 at both temperatures (Table 1). This is in contrast to what was found in the simulations, as the $H_2$ uptakes derived from using the BSSP model in ZIF-68 and ZIF-69 at 77 K and 0.10 atm have the inverse relationship with values of 4.8 and 4.4 mg $g^{-1}$, respectively. This discrepancy is related to the fact that simulations using this polarizable potential in ZIF-68 produced an isotherm that is in outstanding agreement with experiment at 77 K (Figure S6(a)), whereas in ZIF-69, the model slightly undersorbs relative to experiment for nearly all pressures considered at this temperature (Figure S12(a)). The latter result could be a consequence of the force field parameters that were derived for ZIF-69. Nevertheless, we believe that our model does a reasonable job of predicting the $H_2$ sorption properties in both ZIFs.

The $Q_{st}$ for $H_2$ in ZIF-68 and ZIF-69 as derived by applying the virial method[37,38] to the corresponding experimental

$H_2$ sorption isotherms at 77 and 87 K are shown in Figure 3. The initial experimental $Q_{st}$ value for both ZIFs was determined to be 8.1 kJ mol$^{-1}$, which is greater than those for some MOFs that contain exposed metal centers,[3] as for example HKUST-1 (6.0–7.0 kJ mol$^{-1}$).[55–60] t can be observed that both ZIFs display very similar $H_2$ $Q_{st}$ values across the considered loading range. The fact that both ZIF-68 and ZIF-69 exhibit essentially the same zero-coverage $Q_{st}$ value suggests that the most favorable $H_2$ binding site in both ZIFs are identical; this conclusion was validated by our molecular simulations described below (see section IIIC).

The $H_2$ $Q_{st}$ values in ZIF-68 and ZIF-69 as obtained from simulations using the polarizable $H_2$ potential are also shown in Figure 3. For both ZIFs, the theoretical $Q_{st}$ values are in excellent agreement with the corresponding experimental quantities at all loadings considered, especially at low loadings. The initial $Q_{st}$ values were calculated to be 8.0 and 7.8 kJ mol$^{-1}$ for ZIF-68 and ZIF-69, respectively. In essence, the simulations were able to reproduce the same general shape of the experimental $Q_{st}$ plots, and were found to be similar for both ZIFs over the considered loading range, which is in agreement with experiment.

The $Q_{st}$ values obtained from simulations using the other three $H_2$ potentials in ZIF-68 and ZIF-69 are shown in the Supporting Information (Figures S6(c) and S12(c)). The DL model produced $Q_{st}$ values that are close to experiment at low loadings in ZIF-68 (Figure S6(c)), but overestimates $Q_{st}$ at higher loadings. However, in ZIF-69, the DL model $Q_{st}$ underestimates experiment at low loadings, but gives slightly greater values than experiment at higher loadings (Figure S12(c)). The BSS model generated $Q_{st}$ values that underestimate experiment at low loadings but are in close agreement with the experimental $Q_{st}$ plot at higher loadings for both ZIFs. Simulations using the Buch potential produced $Q_{st}$ values that are notably lower than those derived from experiment for all loadings considered in both ZIFs. However, the initial $H_2$ $Q_{st}$ values for the Buch model in ZIF-68 and ZIF-69 are about 6.4 and 6.3 kJ mol$^{-1}$, respectively. The high magnitude of these values suggests that a large portion of $H_2$ adsorbing at the primary binding site in both ZIFs may be attributed to repulsion/dispersion interactions. Nevertheless, the inclusion of explicit polarization interactions as observed in the $Q_{st}$ for the BSSP potential, was necessary to reproduce the experimental initial $Q_{st}$ values for both ZIF-68 and ZIF-69 by our classical GCMC simulations.

### B. Inelastic Neutron Scattering Spectra

The INS spectra for $H_2$ sorbed in ZIF-68 and ZIF-69 at a loading of 2 $H_2$ molecules per formula unit exhibit a wide range of broad features starting at approximately 4 meV (Figure 4). One such band could be observed from about 4–7.5 meV in the INS spectrum for both ZIFs. We may attribute this excitation to $H_2$ located at the strongest adsorption sites in these materials since it is the lowest energy peak in the spectrum, i.e. has the lowest tunneling frequency, and hence displays the largest barrier to rotation. The range of energy transfer values for these rotational tunnelling transitions is lower than those of the lowest energy peaks observed in the INS spectra for most MOFs that contain $[Cu_2(O_2CR)_4]$ clusters.[61–64] This suggests that there is a $H_2$ sorption site present in ZIF-68 and ZIF-69 with a higher barrier to rotation than that at the exposed $Cu^{2+}$ ions in MOFs that contain copper paddlewheels.

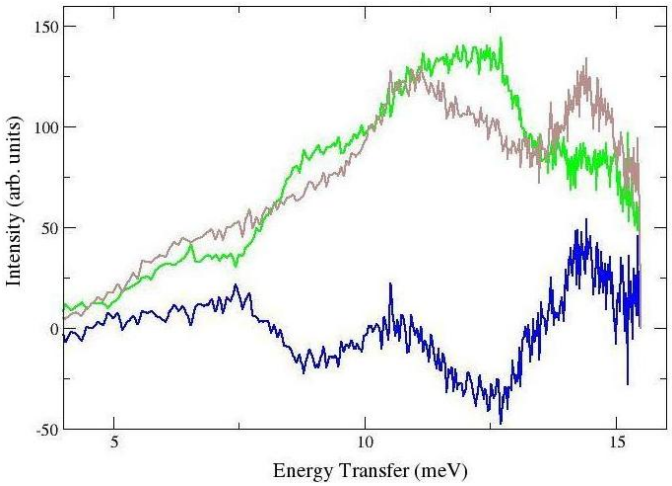


**Figure 4.** Inelastic neutron scattering (INS) spectra for $H_2$ in ZIF-68 (green) and ZIF-69 (brown) at a loading of 2 $H_2$ molecules per formula unit. The difference spectrum between ZIF-68 and ZIF-69 is shown in blue.

The similarity of the INS spectra for both ZIFs is indicated by the difference spectrum shown in Figure 4. While broad INS spectra have been observed for $H_2$ sorbed in certain materials,[64–69] such materials are known to contain extra-framework counterions. Since the framework of ZIF-68 and ZIF-69 is not charged, the broad features of the INS spectrum for these ZIFs represent an unexpected finding. Nonetheless, the widths of the features in INS spectrum for ZIF-68 and ZIF-69 could suggest that there is a distribution of $H_2$ molecule positions and orientations about each unique sorption site in the respective ZIFs.[65,70]

### C. $H_2$ Sorption Sites

Our molecular simulations have provided insights in the binding sites for $H_2$ in ZIF-68 and ZIF-69. Figure 5 shows a distribution of the sites occupied by $H_2$ in ZIF-68 as determine from the simulations. Note, a very similar distribution of sites was observed for $H_2$ sorption in ZIF-69 (see Supporting Information, Figure S13). While the results for the polarizable $H_2$ potential are shown here, we note that the other three $H_2$ models were able to capture the same distribution of adsorption sites in simulation. Three distinct $H_2$ binding sites were found in the simulations in both ZIFs as shown in Figure 5.

The most energetically favorable binding site in both ZIFs (orange colored occupancy in Figure 5), denoted as site 1 in this work, corresponds to $H_2$ located within a confined region between two adjacent 2-nitroimidazolate linkers. Specifically, the $H_2$ molecule is sorbed between the imidazolate groups of these linkers. Close-up views of this binding site in ZIF-68 as obtained from the Monte Carlo adsorption history are shown in Figure 6. Identical views for the analogous site in ZIF-69 are shown in the Supporting Information (Figure S14). It can be observed that each H atom of the adsorbate molecule interacts favorably with the aromatic ring of the 2-nitroimidazolate linkers, particularly with the negatively charged N atoms of the imidazolate groups. The H–N distances were determined to be 3.05, 3.05, 3.13, and 3.15

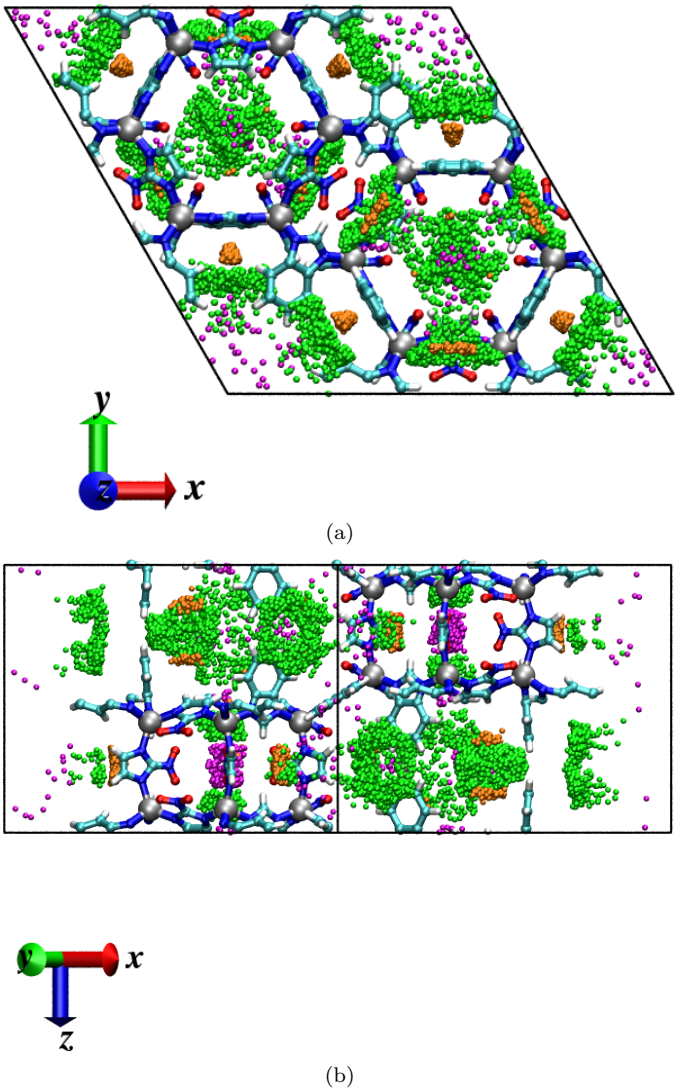


**Figure 5.** **(a)** The $c$-axis view and **(b)** the view of the 45° angle between the $a$ and $b$ axes of the unit cell of ZIF-68 showing the sites of $H_2$ occupancy. Both views are orthographic projections. Orange colored occupancy corresponds to site 1, green colored corresponds to site 2, and magenta colored occupancy corresponds to site 3. The sorption sites in ZIF-69 are very similar (see Supporting Information, Figure S13). Atom colors: C = cyan, H = white, N = blue, O = red, Zn = silver.

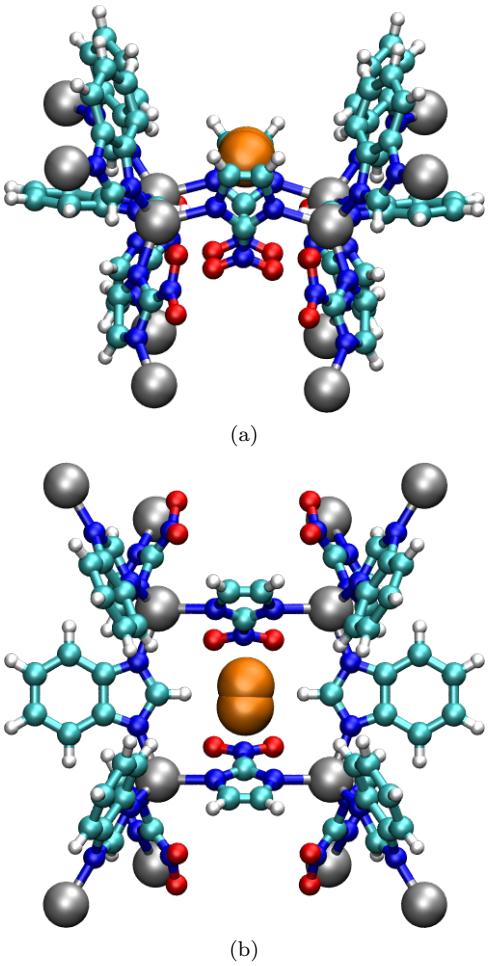


**Figure 6.** Molecular illustration of an adsorbed $H_2$ molecule about the primary binding site in ZIF-68 as determined by simulated annealing: **(a)** side view; **(b)** up view. The sorbate molecule is shown in orange. The primary adsorption site is the region between two imidazolate groups of neighboring 2-nitroimidazolate linkers. A similar primary adsorption site was observed in ZIF-69 (see Supporting Information, Figure S14). Atom colors: C = cyan, H = white, N = blue, O = red, Zn = silver.

Å for the most optimized position of the $H_2$ molecule about this site in ZIF-68 (Figure S8(c)), which was obtained by a simulated annealing Monte Carlo process. The analogous distances in ZIF-69 were found to be 3.22, 3.30, 3.25, and 3.29 Å (Figure S14(c)). From a quantum mechanical point of view, we may suggest that a favorable interaction exists between the $1s$ orbitals of the H atoms and the $2p$ orbitals of the aromatic rings.

The adsorption of $H_2$ between two neighboring 2-nitroimidazolate linkers in ZIF-68 and ZIF-69 corresponds to the experimental zero-loading value of $Q_{st}$ for both ZIFs. This finding was confirmed by canonical Monte Carlo (CMC) simulation studies for a single BSSP $H_2$ molecule within the individual ZIF. The nature of this binding site also explains why the experimental initial $Q_{st}$ values in both ZIFs are similar to each other. It would appear that the presence of the electronegative Cl atom in ZIF-69 does not play much of a role for $H_2$ adsorption. This finding is in stark contrast to what was observed for adsorption of $CO_2$ in these ZIFs, where it was demonstrated that ZIF-69 has greater $CO_2$ uptake and selectivity than ZIF-68.[14,28] Finally, we note that the primary adsorption site identified for the two ZIFs from our simulations is similar to the preferential $H_2$ binding site observed in ZIF-8 by NPD studies, which found that the $H_2$ molecules adsorb onto the imidazolate linkers in the material.[19]

The energetic terms for $H_2$ adsorbed at site 1 in ZIF-68 and ZIF-69 for simulations using the polarizable $H_2$ model can be decomposed to show that repulsion/disperion interactions contribute to roughly 81% and 82% of the total energy, respectively, for binding at this site (Table 2). The constricted region between the two 2-nitroimidazolate linkers is therefore dominated by van der Waals interactions, and this allows the $H_2$ molecule to interact with multiple atoms of the nearby linkers through conformal repulsion/dispersion energetics. This result could explain why the single–site Buch model produced sufficiently high initial $Q_{st}$ values in simulations within the respective ZIFs even though such values notably underestimate the corresponding experimental quantities (Figure S6(c) and S12(c)).

Permanent electrostatic interactions contribute to nearly 9% and 3% of the total energy for $H_2$ sorbing at site 1 in

**Table 2.** The averaged contribution of the energy components from canonical Monte Carlo (CMC) simulations of a single $H_2$ molecule adsorbed at site 1 in ZIF-68 and ZIF-69 using the polarizable $H_2$ potential. The percentage of the total energy and the absolute magnitude (in K) of the energy components are listed. $U_{rd}$, $U_{es}$, and $U_{pol}$ represent the repulsion/dispersion, stationary electrostatic, and many-body polarization energy, respectively.

| $U$ Contribution | ZIF-68 | ZIF-69 |
|---|---|---|
| $U_{rd}$ (%) | 81.3 | 82.0 |
| $U_{es}$ (%) | 8.5 | 2.9 |
| $U_{pol}$ (%) | 10.2 | 15.1 |
| $U_{rd}$ (K) | -783.36 | -800.17 |
| $U_{es}$ (K) | -82.18 | -28.48 |
| $U_{pol}$ (K) | -98.27 | -147.71 |

ZIF-68 and ZIF-69, respectively, which is the smallest contribution of the energetic terms in both ZIFs (Table 2). When comparing the $Q_{st}$ values that were generated using the BSS model to those obtained using the Buch model in both ZIFs, it can be observed that the inclusion of stationary electrostatic interactions increases the initial $Q_{st}$ value in the two ZIFs only slightly, as this was insufficient for reproducing the experimental zero-coverage $Q_{st}$ values (Figures S6(c) and S12(c)). The polarization energy, however, represents approximately 10% and 15% of the total energy for $H_2$ sorbing at site 1 in the respective ZIFs. The inclusion of this interaction was necessary to obtain initial $Q_{st}$ values in agreement with experiment for both ZIFs. A comparison of the $Q_{st}$ values obtained from simulation using the BSSP and BSS models in both ZIFs reveals that the initial $Q_{st}$ values increase from 6.9 to 8.0 kJ mol$^{-1}$ in ZIF-68 (Figure S6(c)) and from 6.4 to 7.8 kJ mol$^{-1}$ in ZIF-69 (Figure S12(c)) when polarization was included.

The next most favorable $H_2$ binding sites in ZIF-68 and ZIF-69 (green colored occupancy in Figure 5) are near the nitro groups of the 2-nitroimidazolate linkers that project into the hexagonal channels of the structures. A large distribution of positions was found for this site. Molecular illustrations for $H_2$ sorbed at this site (denoted site 2) in both ZIFs are shown in the Supporting Information (Figures S9 and S15). The $H_2$ molecule binds to only one side of the nitro group, where a favorable interaction exists between the positively charged H atom and the negatively charged O atom. The $H_2$ molecule at this site can also interact with the nearby imidazolate group of a 2-nitroimidazolate linker, which results in a favorable interaction with the framework.

The tertiary binding sites for the $H_2$ molecules in ZIF-68 and ZIF-69 are indicated by magenta colored occupancy in Figure 5. Close-up views of this binding site in both ZIFs are provided in the Supporting Information (Figure S10 and S16). This site (denoted site 3) also involves binding of $H_2$ onto the nitro groups of the 2-nitroimidazolate linkers, but unlike site 2, the $H_2$ molecule interacts with both oxygen atoms of the nitro groups for this site. As a result, the $H_2$ molecule is now farther away from the proximal imidazolate group of a 2-nitroimidazolate linker. This configuration of the $H_2$ molecule about the nitro groups is therefore less favorable compared to that for site 2, as suggested by the energies obtained from CMC simulation and the two-dimensional quantum rotational levels for $H_2$ adsorbed at the respective sites described below.

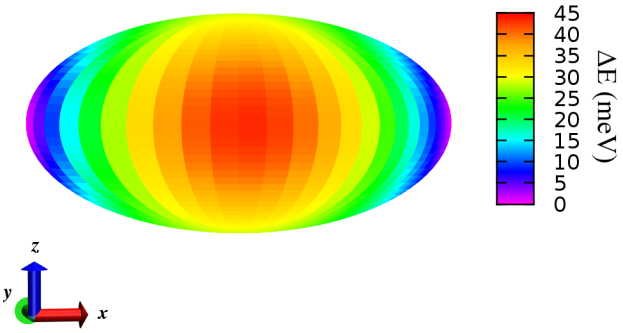


**Figure 7.** Two-dimensional rotational potential energy surface projected onto a sphere for a $H_2$ molecule sorbed about site 1 in ZIF-68 as shown in Figure 6. Relative energies are given in meV. The rotational barrier was calculated to be 43.35 meV.

### D. Rotational Dynamics

Two-dimensional quantum rotational levels for $H_2$ adsorbed at the three binding sites sites in ZIF-68 and ZIF-69 are given in the Supporting Information (Tables S8 and S9). This type of calculation was previously used to predict the rotational transitions for $H_2$ sorbed in various MOFs.[52,53,69,71–78] Here, the results are discussed for calculations using the polarizable $H_2$ potential. For $H_2$ sorbed at site 1 in ZIF-68, a rotational energy level of 6.95 meV was calculated for the transition between $j = 0$ and the lowest $j = 1$ sublevel (Table S8). This calculated transition falls within the range of energies that is associated with the peak from 4–7.5 meV in the INS spectrum for the ZIF (Figure 4). We therefore predict that this peak in the INS spectrum for ZIF-68 corresponds to the sorption of $H_2$ at site 1 in the material. Further, we emphasize that the calculated transition is lower (and hence the higher rotational barrier) than the energy transfer values for the lowest energy peaks observed in the INS spectra for several MOFs that possess open-metal sites, including Co-MOF-74[79] and Zn-MOF-74,[53,80] and those that contain copper paddlewheel clusters.[61–64]

The rotational PES for $H_2$ adsorbed at site 1 in ZIF-68 is displayed in Figure 7, where the reorientation of the $H_2$ molecule by 180° between the minima (shown in violet) over the barriers in between can be observed. The rotational barrier, which corresponds to the maximum on the PES, was determined to be 43.35 meV (or about 1 kcal mol$^{-1}$), which is quite high for a material that does not contain open-metal sites. It is therefore evident that the compact region between the two adjacent 2-nitroimidazolate linkers gives rise to a large degree of hindrance to the reorientation of the adsorbed $H_2$ molecule. In fact, this value for the rotational barrier is greater than those for a number of MOFs that possess open-metal sites based on a literature survey of previous INS and quantum dynamics studies of $H_2$ sorbed in such materials.[75]

For $H_2$ adsorbed at the same site in ZIF-69, however, an energy of 8.24 meV was calculated for the $j = 0$ to $j = 1$ transition, which is 1.29 meV higher than that in ZIF-68 (Table S9). It appears that the energetics for $H_2$ bound at site 1 in ZIF-68 is greater than that for the analogous site in ZIF-69, which in turn is qualitatively consistent with the fact that the theoretical initial $Q_{st}$ values for the two ZIFs is higher for ZIF-68 relative to ZIF-69 (8.0 vs. 7.8 kJ mol$^{-1}$; Figure 3). This could be due to the fact that the region between the two neighboring 2-nitroimidazolate linkers in ZIF-69 is less optimal for the $H_2$ molecules than in the case of

ZIF-68. We note that the distance between two analogous imidazolate N atoms of the nearby 2-nitroimidazolate linkers in this region is 5.95 and 6.24 Å for ZIF-68 and ZIF-69, respectively. It seems that the presence of the Cl atom on the 5-chlorobenzimidazolate linker, which results in a long C–Cl bond, causes the two 2-nitroimidazolate linkers encompassing site 1 to be farther apart in ZIF-69. At the minimum energy positions for $H_2$ sorbed at site 1 in both ZIFs, the H–N distances are slightly longer in ZIF-69, which implies somewhat weaker interactions (Figures S8(c) and S14(c)).

Although the calculated transition of 8.24 meV for $H_2$ sorbed at site 1 in ZIF-69 falls outside the range of energies for the lowest energy peak in the observed INS spectrum (*ca.* 4–7.5 meV), the region between the two neighboring 2-nitroimidazolate linkers still represents the most favorable sorption site for the $H_2$ molecules in this ZIF as determined from GCMC simulations. Thus, the peak from 4–7.5 meV in the INS spectrum for ZIF-69 should correspond to $H_2$ sorbed at site 1 in this material. The higher than expected calculated value of the $j = 0$ to $j = 1$ transition for $H_2$ sorbed at site 1 in ZIF-69 could result from the theoretical potential energy surface for the adsorbent or the lack of coupling to translational motion, which has shown to be important in certain cases.[71] We emphasize again that the region between the two adjacent 2-nitroimidazolate linkers in ZIF-69 imposes a high barrier to rotation on the $H_2$ molecule as in ZIF-68. A rotational barrier of 39.38 meV was calculated for $H_2$ sorbed at site 1 in ZIF-69 (Figure S17), which is also greater than those for many MOFs according to previous INS studies.[75]

For $H_2$ adsorbed at sites 2 and 3 in ZIF-68, the energies of the lowest $j = 0$ to $j = 1$ transition were calculated to be 8.61 and 8.74 meV, respectively (Table S8). These transitions are based on the most favorable location of the $H_2$ molecule for the respective sites based on CMC simulations. Higher transition energies calculated for $H_2$ adsorbed at these sites relative to site 1 indicate that the interaction with $H_2$ is in fact weaker. In addition, since a higher rotational transition was calculated for site 3, this implies that sorption at site 3 is less favorable than at site 2. The broad intensity observed in the range 7.5–10 meV in the INS spectrum should therefore represent $H_2$ binding at these sites in ZIF-68, as the calculated values for the $j = 0$ to $j = 1$ transition for both sites fall within this range of energies. We note that different positions and angular orientations can be observed for $H_2$ adsorbing at these sites, which may give rise to slightly different barriers to rotation. This could explain why this peak appears rather broad in the INS spectrum for both ZIFs.[65,70] The corresponding transitions for the analogous sites in ZIF-69 were calculated to be 11.66 and 13.38 meV, respectively (Table S9). These transitions are notably higher than those for the same sites in ZIF-68, which may be attributed to some inadequacies in the the nature of the PES.

## IV. CONCLUSION

We presented a joint experimental and theoretical study of the adsorption of $H_2$ in ZIF-68 and ZIF-69. This study includes for the first time the experimental $H_2$ adsorption properties in both ZIFs as well as the corresponding INS spectra for $H_2$ adsorbed in these materials. The experimental $H_2$ adsorption isotherms at 77 and 87 K and $Q_{st}$ values in ZIF-68 and ZIF-69 were found to be very similar to each other. The initial $Q_{st}$ value in both ZIFs was determined to be 8.1 kJ mol$^{-1}$, which is comparable to those for MOFs that contain open-metal sites.[3] GCMC simulations of $H_2$ adsorption in ZIF-68 and ZIF-69 confirmed the similarity of the $H_2$ sorption properties for the two ZIFs, with the results from the simulations in excellent agreement with experiment when using a polarizable force field.

It was discovered through the simulations that the most favorable $H_2$ sorption site in both ZIFs corresponds to a confined region between two neighboring 2-nitroimidazolate linkers. In this area in both ZIFs, the $H_2$ molecule can interact favorably with the surrounding imidazolate groups of the linkers. The presence of this site in both ZIFs explains why the two ZIFs have essentially the same zero-loading $H_2$ $Q_{st}$ value despite the fact that one of the ZIFs contain an enhanced functionality through the Cl atom. Our simulations do suggest that $H_2$ sorption is somewhat preferential in ZIF-68, however, which is most likely due to the fact that the region between the two adjacent 2-nitroimidazolate linkers is more constricted in ZIF-68, and thereby allows for greater interactions with the $H_2$ molecules. The presence of the Cl atoms in ZIF-69 appears to have a negligible effect on $H_2$ sorption affinity and capacity, which is in stark contrast to what was observed in the case of $CO_2$ adsorption and separation.[14,28]

The adsorption of $H_2$ at the most favorable binding site in ZIF-68 and ZIF-69 was shown from our simulations to be dominated by van der Waals interactions. However, the addition of stationary electrostatic and many-body polarization interactions was necessary to reproduce the experimental values for the initial $Q_{st}$ value in both ZIFs by our classical GCMC simulation. This demonstrates the importance of using sophisticated modeling techniques to accurately describe the energetics of $H_2$ sorption in ZIFs and related materials. Further, the region between the two neighboring 2-nitroimidazolate linkers was shown to give rise to a high barrier to rotation for the $H_2$ molecules in ZIF-68 and ZIF-69. Calculated rotational barriers for $H_2$ at these sites in both ZIFs are greater than those for numerous extant MOFs, even those that possess open-metal sites.[75]

The INS spectra for $H_2$ adsorbed in ZIFs are also reported for the first time in this work. The INS spectra for $H_2$ in ZIF-68 and ZIF-69 show unusually broad bands, which could be due to the fact that there is a distribution of $H_2$ molecule positions and angular orientations associated with each of the identified sites. Two-dimensional quantum rotation calculations about the binding sites in both ZIFs resulted in $j = 0$ to $j = 1$ transitions that are within a specific range of energies that are observed in the INS spectrum for the respective ZIFs.

The primary $H_2$ sorption site identified for ZIF-68 and ZIF-69 in this work suggests that tuning the organic linker can play a role for increasing the $H_2$ adsorption enthalpy in MOFs and related porous materials through confinement effects. It had been shown that functionalization of the ligand in MOFs can result in higher $H_2$ uptake and $Q_{st}$ values,[58,81] although such an effect was not observed here when comparing the $H_2$ sorption properties for ZIF-68 and ZIF-69. The geometry of the organic ligand used to construct a MOF can also affect the topology of the assembled structure, which in turn could result in the formation of exclusive binding sites in the material. ZIF-68 and ZIF-69 are materials that exhibit a rare **gme** topology as a result of being synthesized using 2-nitroimidazolate and benzimidazolate-type ligands.

The structure of these ZIFs consists of a unique arrangement of the linkers that gives rise to the primary $H_2$ sorption site in both ZIFs.

ZIFs are materials that exhibit exceptional chemical and thermal stability due to the presence of saturated metal centers.[12,14] Unlike MOFs that contain open-metal sites, ZIFs have been shown to display stability after exposure to moisture since the tetrahedral metal nodes cannot coordinate to water molecules. As a result, the pores of ZIFs are more hydrophobic than those for MOFs that contain open-metal sites. As observed in this work, ZIFs can consist of a $H_2$ sorption site that is comparable in energetics to an open-metal site. Thus, ZIFs have promising potential for applications in $H_2$ storage since they can display high $H_2$ uptake and exhibit remarkable stability. It appears that $H_2$ sorption in ZIFs is mostly governed by binding onto the imidazolate-type ligands. Such an interaction is strong if the $H_2$ molecules can interact with multiple imidazolate groups in a constricted region simulatenously, similar to what was observed for the primary $H_2$ binding site for ZIF-68 and ZIF-69 in this work. One may expect that the inclusion of counterions in ZIFs in some fashion would result in an increase in the $H_2$ adsorption enthalpy.

## ASSOCIATED CONTENT

**Supporting Information.** Details of electronic structure calculations, grand canonical Monte Carlo methods, and quantum rotation calculations, pictures of ZIF fragments, tables of properties, and simulated $H_2$ sorption results. This material is available free of charge *via* the Internet at http://pubs.acs.org.

## AUTHOR INFORMATION

**Corresponding Author**
*E-mail: brian.b.space@gmail.com (B.S.)
*E-mail: juergen@usf.edu (J.E.)
**Author Contributions**
§Authors contributed equally
**Notes**
The authors declare no competing financial interest.

## ACKNOWLEDGMENTS

B.S. acknowledges the National Science Foundation (Award No. CHE-1152362), including support from the Major Research Instrumentation Program (Award No. CHE-1531590), the computational resources that were made available by a XSEDE Grant (No. TG-DMR090028), and the use of the services provided by Research Computing at the University of South Florida. We thank Dr. Rahul Banerjee for preparing a sample of ZIF-68 and ZIF-69 and Professor Omar M. Yaghi for graciously allowing us to use his adsorption instrument.

[1] Zhao, D.; Yuan, D.; Zhou, H.-C. The current status of hydrogen storage in metal–organic frameworks. *Energy Environ. Sci.* **2008**, *1*, 222–235.

[2] Collins, D. J.; Ma, S.; Zhou, H.-C. *Metal-Organic Frameworks: Design and Application*; John Wiley & Sons, Inc.: Hoboken, NJ, 2010; pp 249–266.

[3] Suh, M. P.; Park, H. J.; Prasad, T. K.; Lim, D.-W. Hydrogen Storage in Metal–Organic Frameworks. *Chem. Rev.* **2012**, *112*, 782–835.

[4] Yaghi, O. M.; Li, H.; Davis, C.; Richardson, D.; Groy, T. L. Synthetic strategies, structure patterns, and emerging properties in the chemistry of modular porous solids. *Acc. Chem. Res.* **1998**, *31*, 474–484.

[5] DOE Targets for Onboard Hydrogen Storage Systems for Light-Duty Vehicles. 2009; `http://www1.eere.energy.gov/hydrogenandfuelcells/storage/pdfs/targets_onboard_hydro_storage.pdf`.

[6] Bhatia, S. K.; Myers, A. L. Optimum Conditions for Adsorptive Storage. *Langmuir* **2006**, *22*, 1688–1700.

[7] Ma, S. Gas adsorption applications of porous metal–organic frameworks. *Pure Appl. Chem.* **2009**, *81*, 2235–2251.

[8] Eddaoudi, M.; Moler, D. B.; Li, H.; Chen, B.; Reineke, T. M.; O'Keeffe, M.; Yaghi, O. M. Modular Chemistry: Secondary Building Units as a Basis for the Design of Highly Porous and Robust Metal–Organic Carboxylate Frameworks. *Acc. Chem. Res.* **2001**, *34*, 319–330, PMID: 11308306.

[9] Eddaoudi, M.; Eubank, J. F. *Metal–Organic Frameworks: Design and Application*; John Wiley & Sons, Inc.: Hoboken, NJ, 2010; pp 37–89.

[10] Liu, Y.; Kravtsov, V. C.; Larsen, R.; Eddaoudi, M. Molecular building blocks approach to the assembly of zeolite-like metal-organic frameworks (ZMOFs) with extra-large cavities. *Chem. Commun.* **2006**, 1488–1490.

[11] Huang, X.-C.; Lin, Y.-Y.; Zhang, J.-P.; Chen, X.-M. Ligand-Directed Strategy for Zeolite-Type Metal–Organic Frameworks: Zinc(II) Imidazolates with Unusual Zeolitic Topologies. *Angew. Chem. Int. Ed.* **2006**, *45*, 1557–1559.

[12] Park, K. S.; Ni, Z.; Côté, A. P.; Choi, J. Y.; Huang, R.; Uribe-Romo, F. J.; Chae, H. K.; OKeeffe, M.; Yaghi, O. M. Exceptional chemical and thermal stability of zeolitic imidazolate frameworks. *Proc. Natl. Acad. Sci. U.S.A.* **2006**, *103*, 10186–10191.

[13] Hayashi, H.; Côté, A. P.; Furukawa, H.; OKeeffe, M.; Yaghi, O. M. Zeolite A imidazolate frameworks. *Nat. Mater.* **2007**, *6*, 501–506.

[14] Banerjee, R.; Phan, A.; Wang, B.; Knobler, C.; Furukawa, H.; O'Keeffe, M.; Yaghi, O. M. High-throughput synthesis of zeolitic imidazolate frameworks and application to $CO_2$ capture. *Science* **2008**, *319*, 939–943.

[15] Wang, B.; Côté, A. P.; Furukawa, H.; OKeeffe, M.; Yaghi, O. M. Colossal cages in zeolitic imidazolate frameworks as selective carbon dioxide reservoirs. *Nature* **2008**, *453*, 207–211.

[16] Banerjee, R.; Furukawa, H.; Britt, D.; Knobler, C.; OKeeffe, M.; Yaghi, O. M. Control of Pore Size and Functionality in Isoreticular Zeolitic Imidazolate Frameworks and their Carbon Dioxide Selective Capture Properties. *J. Am. Chem. Soc.* **2009**, *131*, 3875–3877, PMID: 19292488.

[17] Phan, A.; Doonan, C. J.; Uribe-Romo, F. J.; Knobler, C. B.; OKeeffe, M.; Yaghi, O. M. Synthesis, Structure, and Carbon Dioxide Capture Properties of Zeolitic Imidazolate Frameworks. *Acc. Chem. Res.* **2010**, *43*, 58–67, PMID: 19877580.

[18] Chen, B.; Yang, Z.; Zhu, Y.; Xia, Y. Zeolitic imidazolate framework materials: recent progress in synthesis and applications. *J. Mater. Chem. A* **2014**, *2*, 16811–16831.

[19] Wu, H.; Zhou, W.; Yildirim, T. Hydrogen Storage in a Prototypical Zeolitic Imidazolate Framework-8. *J. Am. Chem. Soc.* **2007**, *129*, 5314–5315, PMID: 17425313.

[20] Li, K.; Olson, D. H.; Seidel, J.; Emge, T. J.; Gong, H.; Zeng, H.; Li, J. Zeolitic Imidazolate Frameworks for Kinetic Separation of Propane and Propene. *J. Am. Chem. Soc.* **2009**, *131*, 10368–10369, PMID: 19722614.

[21] Morris, W.; Leung, B.; Furukawa, H.; Yaghi, O. K.; He, N.; Hayashi, H.; Houndonougbo, Y.; Asta, M.; Laird, B. B.; Yaghi, O. M. A Combined Experimental–Computational Investigation of Carbon Dioxide Capture in a Series of Isoreticular Zeolitic Imidazolate Frameworks. *J. Am. Chem. Soc.* **2010**, *132*, 11006–11008, PMID: 20698658.

[22] Pérez-Pellitero, J.; Amrouche, H.; Siperstein, F. R.; Pirngruber, G.; Nieto-Draghi, C.; Chaplais, G.; Simon-Masseron, A.; Bazer-Bachi, D.; Peralta, D.; Bats, N. Adsorption of $CO_2$, $CH_4$, and $N_2$ on zeolitic imidazolate frameworks: experiments and simulations. *Chem. Eur. J.* **2010**, *16*, 1560–1571.

[23] Amrouche, H.; Aguado, S.; Pérez-Pellitero, J.; Chizallet, C.; Siperstein, F.; Farrusseng, D.; Bats, N.; Nieto-Draghi, C. Experimental and Computational Study of Functionality Impact on Sodalite–Zeolitic Imidazolate Frameworks for $CO_2$ Separation. *J. Phys. Chem. C* **2011**, *115*, 16425–16432.

[24] Houndonougbo, Y.; Signer, C.; He, N.; Morris, W.; Furukawa, H.; Ray, K. G.; Olmsted, D. L.; Asta, M.; Laird, B. B.; Yaghi, O. M. A Combined Experimental–Computational Investigation of Methane Adsorption and Selectivity in a Series of Isoreticular Zeolitic Imidazolate Frameworks. *J. Phys. Chem. C* **2013**, *117*, 10326–10335.

[25] Liu, D.; Zheng, C.; Yang, Q.; Zhong, C. Understanding the Adsorption and Diffusion of Carbon Dioxide in Zeolitic Imidazolate Frameworks: A Molecular Simulation Study. *J. Phys. Chem. C* **2009**, *113*, 5004–5009.

[26] Rankin, R. B.; Liu, J.; Kulkarni, A. D.; Johnson, J. K. Adsorption and Diffusion of Light Gases in ZIF-68 and ZIF-70: A Simulation Study. *J. Phys. Chem. C* **2009**, *113*, 16906–16914.

[27] Zhou, M.; Wang, Q.; Zhang, L.; Liu, Y.-C.; Kang, Y. Adsorption Sites of Hydrogen in Zeolitic Imidazolate Frameworks. *J. Phys. Chem. B* **2009**, *113*, 11049–11053, PMID: 19624113.

[28] Liu, B.; Smit, B. Molecular Simulation Studies of Separation of $CO_2/N_2$, $CO_2/CH_4$, and $CH_4/N_2$ by ZIFs. *J. Phys. Chem. C* **2010**, *114*, 8515–8522.

[29] Sirjoosingh, A.; Alavi, S.; Woo, T. K. Grand-Canonical Monte Carlo and Molecular-Dynamics Simulations of Carbon-Dioxide and Carbon-Monoxide Adsorption in Zeolitic Imidazolate Framework Materials. *J. Phys. Chem. C* **2010**, *114*, 2171–2178.

[30] Liu, Y.; Liu, H.; Hu, Y.; Jiang, J. Density Functional Theory for Adsorption of Gas Mixtures in Metal–Organic Frameworks. *J. Phys. Chem. B* **2010**, *114*, 2820–2827, PMID: 20143831.

[31] Guo, H.-c.; Shi, F.; Ma, Z.-f.; Liu, X.-q. Molecular Simulation for Adsorption and Separation of $CH_4/H_2$ in Zeolitic Imidazolate Frameworks. *J. Phys. Chem. C* **2010**, *114*, 21891–21891.

[32] Ray, K. G.; Olmsted, D. L.; Houndonougbo, Y.; Laird, B. B.; Asta, M. Origins of $CH_4/CO_2$ Adsorption Selectivity in Zeolitic Imidazolate Frameworks: A van der Waals Density Functional Study. *J. Phys. Chem. C* **2013**, *117*, 14642–14651.

[33] Prakash, M.; Sakhavand, N.; Shahsavari, R. $H_2$, $N_2$, and $CH_4$ Gas Adsorption in Zeolitic Imidazolate Framework-95 and -100: Ab Initio Based Grand Canonical Monte Carlo Simulations. *J. Phys. Chem. C* **2013**, *117*, 24407–24416.

[34] Ray, K. G.; Olmsted, D. L.; Burton, J. M. R.; Houndonougbo, Y.; Laird, B. B.; Asta, M. Gas Membrane Selectivity Enabled by Zeolitic Imidazolate Framework Electrostatics. *Chem. Mater.* **2014**, *26*, 3976–3985.

[35] Eckert, J.; Lohstroh, W. In *Neutron Applications in Materials for Energy*; Kearley, G. J., Peterson, V. K., Eds.; Neutron Scattering Applications and Techniques; Springer International Publishing, 2015; pp 205–239.

[36] Pham, T.; Forrest, K. A.; Space, B.; Eckert, J. Dynamics of $H_2$ adsorbed in porous materials as revealed by computational

analysis of inelastic neutron scattering spectra. *Phys. Chem. Chem. Phys.* **2016**, *18*, 17141–17158.

[37] Czepirski, L.; JagieŁŁo, J. Virial-type thermal equation of gas–solid adsorption. *Chem. Eng. Sci.* **1989**, *44*, 797–801.

[38] Dincă, M.; Dailly, A.; Liu, Y.; Brown, C. M.; Neumann, D. A.; Long, J. R. Hydrogen Storage in a Microporous Metal–Organic Framework with Exposed $Mn^{2+}$ Coordination Sites. *J. Am. Chem. Soc.* **2006**, *128*, 16876–16883.

[39] Metropolis, N.; Rosenbluth, A. W.; Rosenbluth, M. N.; Teller, A. H.; Teller, E. Equation of state calculations by fast computing machines. *J. Chem. Phys.* **1953**, *21*, 1087–1092.

[40] Kirkpatrick, S.; Gelatt, C. D.; Vecchi, M. P. Optimization by simmulated annealing. *Science* **1983**, *220*, 671–680.

[41] Ewald, P. P. Die Berechnung optischer und elektrostatischer Gitterpotentiale. *Ann. Phys.* **1921**, *369*, 253–287.

[42] Wells, B. A.; Chaffee, A. L. Ewald Summation for Molecular Simulations. *J. Chem. Theory Comput.* **2015**, *11*, 3684–3695, PMID: 26574452.

[43] Applequist, J.; Carl, J. R.; Fung, K.-K. Atom dipole interaction model for molecular polarizability. Application to polyatomic molecules and determination of atom polarizabilities. *J. Am. Chem. Soc.* **1972**, *94*, 2952–2960.

[44] Thole, B. Molecular polarizabilities calculated with a modified dipole interaction. *Chem. Phys.* **1981**, *59*, 341–350.

[45] Bode, K. A.; Applequist, J. A New Optimization of Atom Polarizabilities in Halomethanes, Aldehydes, Ketones, and Amides by Way of the Atom Dipole Interaction Model. *J. Phys. Chem.* **1996**, *100*, 17820–17824.

[46] McLaughlin, K.; Cioce, C. R.; Pham, T.; Belof, J. L.; Space, B. Efficient calculation of many-body induced electrostatics in molecular systems. *J. Chem. Phys.* **2013**, *139*, 184112.

[47] Feynman, R. P.; Hibbs, A. R. *Quantum Mechanics and Path Integrals*; McGraw-Hill: New York, 1965; pp. 281.

[48] Buch, V. Path integral simulations of mixed para-$D_2$ and ortho-$D_2$ clusters: The orientational effects. *J. Chem. Phys.* **1994**, *100*, 7610–7629.

[49] Darkrim, F.; Levesque, D. Monte Carlo simulations of hydrogen adsorption in single-walled carbon nanotubes. *J. Chem. Phys.* **1998**, *109*, 4981–4984.

[50] Belof, J. L.; Stern, A. C.; Space, B. An Accurate and Transferable Intermolecular Diatomic Hydrogen Potential for Condensed Phase Simulation. *J. Chem. Theory Comput.* **2008**, *4*, 1332–1337.

[51] Garberoglio, G.; Skoulidas, A. I.; Johnson, J. K. Adsorption of Gases in Metal Organic Materials: Comparison of Simulations and Experiments. *J. Phys. Chem. B* **2005**, *109*, 13094–13103, PMID: 16852629.

[52] Pham, T.; Forrest, K. A.; McLaughlin, K.; Eckert, J.; Space, B. Capturing the $H_2$–Metal Interaction in Mg-MOF-74 Using Classical Polarization. *J. Phys. Chem. C* **2014**, *118*, 22683–22690.

[53] Pham, T.; Forrest, K. A.; Banerjee, R.; Orcajo, G.; Eckert, J.; Space, B. Understanding the $H_2$ Sorption Trends in the M-MOF-74 Series (M = Mg, Ni, Co, Zn). *J. Phys. Chem. C* **2015**, *119*, 1078–1090.

[54] Forrest, K. A.; Pham, T.; Georgiev, P. A.; Pinzan, F.; Cioce, C. R.; Unruh, T.; Eckert, J.; Space, B. Investigating $H_2$ Sorption in a Fluorinated Metal–Organic Framework with Small Pores Through Molecular Simulation and Inelastic Neutron Scattering. *Langmuir* **2015**, *31*, 7328–7336, PMID: 26083895.

[55] Lee, J.; Li, J.; Jagiello, J. Gas sorption properties of microporous metal organic frameworks. *J. Solid State Chem.* **2005**, *178*, 2527–2532.

[56] Krawiec, P.; Kramer, M.; Sabo, M.; Kunschke, R.; Fröde, H.; Kaskel, S. Improved Hydrogen Storage in the Metal–Organic Framework $Cu_3(BTC)_2$. *Adv. Eng. Mater.* **2006**, *8*, 293–296.

[57] Panella, B.; Hirscher, M.; Pütter, H.; Müller, U. Hydrogen Adsorption in Metal–Organic Frameworks: Cu-MOFs and Zn-MOFs Compared. *Adv. Funct. Mater.* **2006**, *16*, 520–524.

[58] Rowsell, J. L. C.; Yaghi, O. M. Effects of Functionalization, Catenation, and Variation of the Metal Oxide and Organic Linking Units on the Low-Pressure Hydrogen Adsorption Properties of Metal–Organic Frameworks. *J. Am. Chem. Soc.* **2006**, *128*, 1304–1315, PMID: 16433549.

[59] Wong-Foy, A. G.; Matzger, A. J.; Yaghi, O. M. Exceptional $H_2$ Saturation Uptake in Microporous Metal–Organic Frameworks. *J. Am. Chem. Soc.* **2006**, *128*, 3494–3495.

[60] Xiao, B.; Wheatley, P. S.; Zhao, X.; Fletcher, A. J.; Fox, S.; Rossi, A. G.; Megson, I. L.; Bordiga, S.; Regli, L.; Thomas, K. M.; Morris, R. E. High-Capacity Hydrogen and Nitric Oxide Adsorption and Storage in a Metal–Organic Framework. *J. Am. Chem. Soc.* **2007**, *129*, 1203–1209, PMID: 17263402.

[61] Brown, C. M.; Liu, Y.; Yildirim, T.; Peterson, V. K.; Kepert, C. J. Hydrogen adsorption in HKUST-1: a combined inelastic neutron scattering and first-principles study. *Nanotechnology* **2009**, *20*, 204025.

[62] Ma, S.; Eckert, J.; Forster, P. M.; Yoon, J. W.; Hwang, Y. K.; Chang, J.-S.; Collier, C. D.; Parise, J. B.; Zhou, H.-C. Further Investigation of the Effect of Framework Catenation on Hydrogen Uptake in Metal–Organic Frameworks. *J. Am. Chem. Soc.* **2008**, *130*, 15896–15902.

[63] Wang, X.-S.; Ma, S.; Forster, P.; Yuan, D.; Eckert, J.; López, J.; Murphy, B.; Parise, J.; Zhou, H.-C. Enhancing $H_2$ Uptake by "Close-Packing" Alignment of Open Copper Sites in Metal–Organic Frameworks. *Angew. Chem. Int. Ed.* **2008**, *47*, 7263–7266.

[64] Eubank, J. F.; Nouar, F.; Luebke, R.; Cairns, A. J.; Wojtas, L.; Alkordi, M.; Bousquet, T.; Hight, M. R.; Eckert, J.; Embs, J. P.; Georgiev, P. A.; Eddaoudi, M. On Demand: The Singular rht Net, an Ideal Blueprint for the Construction of a Metal–Organic Framework (MOF) Platform. *Angew. Chem. Int. Ed.* **2012**, *51*, 10099–10103.

[65] MacKinnon, J. A.; Eckert, J.; Coker, D. F.; Bug, A. L. R. Computational study of molecular hydrogen in zeolite NaA. II. Density of rotational states and inelastic neutron scattering spectra. *J. Chem. Phys.* **2001**, *114*, 10137–10150.

[66] Liu, Y.; Eubank, J. F.; Cairns, A. J.; Eckert, J.; Kravtsov, V. C.; Luebke, R.; Eddaoudi, M. Assembly of Metal–Organic Frameworks (MOFs) Based on Indium–Trimer Building Blocks: A Porous MOF with soc Topology and High Hydrogen Storage. *Angew. Chem. Int. Ed.* **2007**, *46*, 3278–3283.

[67] Nouar, F.; Eckert, J.; Eubank, J. F.; Forster, P.; Eddaoudi, M. Zeolite-like Metal–Organic Frameworks (ZMOFs) as Hydrogen Storage Platform: Lithium and Magnesium Ion-Exchange and $H_2$-(*rho*-ZMOF) Interaction Studies. *J. Am. Chem. Soc.* **2009**, *131*, 2864–2870, PMID: 19206515.

[68] Eckert, J.; Trouw, F. R.; Mojet, B.; Forster, P.; Lobo, R. Interaction of Hydrogen with Extraframework Cations in Zeolite Hosts Probed by Inelastic Neutron Scattering Spectroscopy. *J. Nanosci. Nanotechnol.* **2010**, *10*, 49–59.

[69] Forrest, K. A.; Pham, T.; Georgiev, P. A.; Embs, J. P.; Waggoner, N. W.; Hogan, A.; Humphrey, S. M.; Eckert, J.; Space, B. Inelastic Neutron Scattering and Theoretical Studies of $H_2$ Sorption in a Dy(III)-Based Phosphine Coordination Material. *Chem. Mater.* **2015**, *27*, 7619–7626.

[70] Anderson, C.-R.; Coker, D. F.; Eckert, J.; Bug, A. L. Computational study of molecular hydrogen in zeolite Na-A. I. Potential energy surfaces and thermodynamic separation factors for ortho and para hydrogen. *J. Chem. Phys.* **1999**, *111*, 7599–7613.

[71] Matanović, I.; Belof, J. L.; Space, B.; Sillar, K.; Sauer, J.; Eckert, J.; Bačić, Z. Hydrogen adsorbed in a metal organic framework-5: Coupled translation-rotation eigenstates from quantum five-dimensional calculations. *J. Chem. Phys.* **2012**, *137*, 014701.

[72] Pham, T.; Forrest, K. A.; Hogan, A.; McLaughlin, K.; Belof, J. L.; Eckert, J.; Space, B. Simulations of Hydrogen Sorption in *rht*-MOF-1: Identifying the Binding Sites Through Explicit Polarization and Quantum Rotation Calculations. *J. Mater. Chem. A* **2014**, *2*, 2088–2100.

[73] Pham, T.; Forrest, K. A.; Eckert, J.; Georgiev, P. A.; Mullen, A.; Luebke, R.; Cairns, A. J.; Belmabkhout, Y.; Eubank, J. F.; McLaughlin, K.; Lohstroh, W.; Eddaoudi, M.; Space, B. Investigating the Gas Sorption Mechanism in an *rht*-Metal–Organic Framework through Computational Studies. *J. Phys. Chem. C* **2014**, *118*, 439–456.

[74] Nugent, P.; Pham, T.; McLaughlin, K.; Georgiev, P. A.; Lohstroh, W.; Embs, J. P.; Zaworotko, M. J.; Space, B.; Eckert, J. Dramatic effect of pore size reduction on the dynamics of hydrogen adsorbed in metal–organic materials. *J. Mater. Chem. A* **2014**, *2*, 13884–13891.

[75] Pham, T.; Forrest, K. A.; Georgiev, P. A.; Lohstroh, W.; Xue, D.-X.; Hogan, A.; Eddaoudi, M.; Space, B.; Eckert, J. A high rotational barrier for physisorbed hydrogen in an fcu-metal–organic framework. *Chem. Commun.* **2014**, *50*, 14109–14112.

[76] Pham, T.; Forrest, K. A.; Hogan, A.; Tudor, B.; McLaughlin, K.; Belof, J. L.; Eckert, J.; Space, B. Understanding Hydrogen Sorption in In-*soc*-MOF: A Charged Metal–Organic Framework with Open-Metal Sites, Narrow Channels, and Counterions. *Cryst. Growth Des.* **2015**, *15*, 1460–1471.

[77] Pham, T.; Forrest, K. A.; Falcão, E. H. L.; Eckert, J.; Space, B. Exceptional $H_2$ sorption characteristics in a $Mg^{2+}$-based metal–organic framework with small pores: insights from experimental and theoretical studies. *Phys. Chem. Chem. Phys.* **2016**, *18*, 1786–1796.

[78] Pham, T.; Forrest, K. A.; Eckert, J.; Space, B. Dramatic Effect of the Electrostatic Parameters on H2 Sorption in an M-MOF-74 Analogue. *Cryst. Growth Des.* **2016**, *16*, 867–874.

[79] Dietzel, P. D. C.; Georgiev, P. A.; Eckert, J.; Blom, R.; Strassle, T.; Unruh, T. Interaction of hydrogen with accessible metal sites in the metal-organic frameworks $M_2$(dhtp) (CPO-27-M; M = Ni, Co, Mg). *Chem. Commun.* **2010**, *46*, 4962–4964.

[80] Liu, Y.; Kabbour, H.; Brown, C. M.; Neumann, D. A.; Ahn, C. C. Increasing the Density of Adsorbed Hydrogen with Coordinatively Unsaturated Metal Centers in Metal–Organic Frameworks. *Langmuir* **2008**, *24*, 4772–4777.

[81] Rowsell, J. L. C.; Millward, A. R.; Park, K. S.; Yaghi, O. M. Hydrogen Sorption in Functionalized Metal–Organic Frameworks. *J. Am. Chem. Soc.* **2004**, *126*, 5666–5667.